NOTICE CONCERNING COPYRIGHT RESTRICTIONS

in the pore spaces not occupied by a wetting fluid (paraffin wax) after solidifying the fluid in place. It is important to recognize that when the rock is partially saturated with hydrocarbon paraffin, clay minerals present in rock pore space are immobilized. Thus formation factor extrapolated to an electrolyte saturation of unity (and paraffin saturation of zero), $F = 18$, corresponds to that of "clean" rock (without clay). Even though the change in the trend of rock electrical conductivity at low electrolyte concentrations represents the contribution to surface conduction due to clays, this component is negligible. Effective formation factor data have been studied in light of the wetting-phase distribution observed at different saturations with the aid of a complete pore cast and its associated rock section. Our analysis shows that (1) ~ 30% of the pore space consists of grain-contact pores (i.e., thin sheets and micropores) and intergranular pores connected by smaller throats, (2) ~ 40% of the pore space consists of intergranular conduits composed of pores connected by larger throats, and (3) ~ 30% of the intergranular pore space remains disconnected. The grain-contact pore space of large surface areas (thin sheets), micropores, and intergranular pores connected by smaller throats provide the ions with important alternative paths to the intergranular conduits connected by larger throats. Therefore, for a consolidated rock such as Berea sandstone, we find no unique relationship between effective formation factor and electrolyte saturation, nor do we find a unique definition of the Archie saturation exponent, n, for the full range of saturation. Finally, the Archie saturation exponent n is found to vary from approximately 3 when connected grain-contact pore space (i.e., thin sheets and micropores) and intergranular pores connected by smaller throats are filled with hydrocarbon paraffin to approximately 5 when intergranular conduits connected by larger throats are filled with hydrocarbon paraffin, with a critical saturation (S_{crit}) of 0.7.

REFERENCES

Anderson, W.G., 1986. Wettability literature survey—Part 3: The effects of wettability on the electrical properties of porous media. J. Pet. Technol., v. 12, p. 1371–1378.

Archie, G.E., 1942. The electrical resistivity log as an aid in determining some reservoir characteristics. Trans. AIME, v. 146, p. 55–62.

Khilar, K.C., and Fogler, H.S., 1984. The existence of a critical salt concentration for particle release. J. Coll. Int. Sci., v. 101, p. 214–224.

Schlueter, E.M., Myer, L.R., Cook, N.G.W., and Witherspoon, P.A., 1992. Formation factor and the microscopic distribution of wetting phase in pore space of Berea sandstone. Lawrence Berkeley Laboratory Report LBL-33207.

Sposito, G., 1984. The Surface Chemistry of Soils. Oxford University Press, New York.

Wyllie, M.R.J., 1963. The Fundamentals of Electric Log Interpretation. Academic Press, Inc., New York.

6814

Predicting the Capillary Pressure of Berea Sandstone from Microgeometry

E. M. Schlueter, R. W. Zimmerman, L. R. Myer, N. G. W. Cook, and P. A. Witherspoon

The macroscopic transport properties of porous (and fractured) media depend sensitively upon processes at the pore level, which are controlled principally by the geometry and connectivity of the pore space. In addition, the microphysical, microchemical, and microbiological processes at the pore level affect both the hydraulic and the electric properties of porous materials. Consequently, there is a need for a basic understanding of how pore morphology and other related factors can be used to predict single and multiphase physical properties of porous media, such as intrinsic permeability, relative permeability, and capillary pressure. Visual observation and analysis of Berea sandstone complete pore structure by means of pore casts reveal that the rock pore space is composed of grain-contact pore space (i.e., thin sheets and micropores) connected to larger intergranular pore segments and pore throats, with the whole structure arranged in a three-dimensional irregular network of irregularly shaped pores (Schlueter et al., 1992a).

In our study, we have attempted to understand, through analysis and experiment, how the relationship between capillary pressure and saturation is controlled by the rock pore structure and the distribution of wetting and nonwetting phases in the pore space. For this purpose, we have made analytical calculations of capillary pressure on the basis of pore microgeometry. As a zero-order approximation, we have idealized the porous medium as consisting of an assembly of parallel capillaries of arbitrary cross sections. The mathematical expression for capillary pressure as a function of saturation depends on the distribution of pore hydraulic radii and the area-perimeter power-law relationship of pores (Schlueter et al., 1992b). Two-dimensional scanning electron

microscope (SEM) photomicrographs of rock cross sections have been employed to measure directly the areas, perimeters, and hydraulic radii of the individual pores. Account is taken of the fact that the cross sections are randomly oriented with respect to the channel axes. The predictions of our model are compared with laboratory capillary pressure curves obtained with a technique using Wood's metal alloy as the nonwetting phase instead of the conventional mercury porosimetry. This technique allows for direct examination and analysis of the fluid distributions in the rock pore space (obtained at fixed pore pressures and saturation levels) after the experiment.

THE MODEL

In two-phase conditions, the capillary pressure between wetting and nonwetting phases in a circular tube of radius r is given by Laplace's equation (Scheidegger, 1974)

$$P_c = \frac{2\varsigma \cos\alpha}{r}, \tag{1}$$

where ς is the surface tension between wetting and nonwetting phases and α the contact angle between the wetting phase meniscus and the tube wall.

If the capillaries are not circular, the equation for the capillary pressure has to be generalized by replacing $2/r$ by $(1/r_1) + (1/r_2)$:

$$P_c = \varsigma\left(\frac{1}{r_1} + \frac{1}{r_2}\right), \tag{2}$$

where r_1 and r_2 are the principal radii of curvature of the meniscus.

If the pore openings are not of a simple geometric form, Eq. (2) is still a valid expression for the capillary pressure. To obtain a theoretical relationship between the saturation and capillary pressure for a porous medium, an analytical expression for the average interfacial curvature as a function of saturation is required. This is a very difficult task.

Schultze (1925a,b) has shown experimentally that the capillary pressures for such capillaries under the assumption of zero contact angle are given approximately by the equation

$$P_c = \frac{\varsigma}{R_H}, \tag{3}$$

where R_H is the ratio of area to perimeter of the capillary. A list of comparative values for testing Eq. (3) is given in Table 1 (Carman, 1941). Since Eq. (3) gives a reasonably accurate prediction of capillary pressure in noncircular capillaries, it can be assumed to be applicable to the capillary channels in a porous medium (Scheidegger, 1974).

In our model, it is assumed that there is no accessibility problem; i.e., regardless of the spatial arrangement of pores, the pores are occupied by the nonwetting phase in the order of largest pores first. Similarly, for the wetting phase, the pores are occupied by the wetting phase in the order of smallest pores first. Therefore, given a hydraulic radius distribution of intergranular pore space $\beta(R_H)$, and assuming that the pores are filled by the wetting phase in ascending order up to a cutoff radius R'_H, we may write the saturation of the wetting phase $S_w(R'_H)$ as (cf. Pruess and Tsang, 1989; Schlueter and Pruess, 1990)

$$S_w(R'_H) = \frac{\int_0^{R'_H} A(R_H)\beta(R_H)dR_H}{\int_0^{\infty} A(R_H)\beta(R_H)dR_H}, \tag{4}$$

where the pore hydraulic radius is defined as the ratio of the pore area A to the pore perimeter P.

Measurements of hydraulic radius of intergranular pore space obtained from two-dimensional SEM photomicrographs of Berea sandstone rock sections have been found to follow a skewed distribution that is well approximated by a log-normal distribution. The log-normal distribution is given by the following expression (hydraulic radius $R_H \geq 0$):

$$\beta(R_H) = \frac{1}{\sqrt{2\pi}\sigma \ln 10}\frac{1}{R_H}\exp\left(\frac{-\left[\log R_H - \log R_{H_0}\right]^2}{2\sigma^2}\right), \tag{5}$$

Table 1. List of comparative values to show equivalence of the reciprocal hydraulic radius ($1/R_H$) and the reciprocal mean radius of curvature $(1/r_1) + (1/r_2)$ in a capillary (r_i is the radius of the inscribed circle).

Cross section	$1/r_1 + 1/r_2$	$1/R_H$
Circle	$2/r$	$2/r$
Parallel plates	$1/b$	$1/b$
Rectangle	$1/a + 1/b$	$1/a + 1/b$
Equilateral triangle	$2/r_i$	$2/r_i$
Square	$2/r_i$	$2/r_i$
Ellipse $a:b = 2:1$	$1.50/b$	$1.20/b$
Ellipse $a:b = 5:1$	$1.10/b$	$1.54/b$
Ellipse $a:b = 10:1$	$1.34/b$	$1.30/b$

Source: After Carman, 1941.

where R_{H_0} is the most probable hydraulic radius and σ the variance. The corresponding mean hydraulic radius R_{H_m} is larger than the most probable hydraulic radius; it is

$$R_{H_m} = R_{H_0} \exp\left(\frac{(\sigma \ln 10)^2}{2}\right) . \tag{6}$$

Invoking the perimeter-area power-law relationship (Schlueter et al., 1992b) gives

$$A = mP^{\gamma} , \tag{7}$$

where log m is the intercept on the log A axis and γ the noninteger slope of the log A – log P plot. The area can be expressed in terms of the hydraulic radius as follows:

$$A(R_H) = m^{1/(1-\gamma)} R_H^{\gamma/(\gamma-1)} . \tag{8}$$

Expressed in terms of the cutoff hydraulic radius, Eq. (4) becomes

$$S_w(R'_H) = \frac{\int_0^{R'_H} R_H^{\gamma/(\gamma-1)} \beta(R_H) dR_H}{\int_0^{\infty} R_H^{\gamma/(\gamma-1)} \beta(R_H) dR_H} . \tag{9}$$

Integrating Eq. (9) yields

$$S_w(R'_H) = \frac{1}{2}\left(1 \pm erf\left[\frac{(\log R'_H - \delta)}{\sqrt{2\sigma^2}}\right]\right) , \tag{10}$$

where the cutoff hydraulic radius is given by

$$R'_H = 10^{\delta - \sqrt{2\sigma^2}\, erfi(1-2S_w)} , \tag{11}$$

where $\delta = \sigma^2 \ln 10 \left[\gamma/(\gamma-1)\right] + \log R_{H_0}$, σ is the variance of log R_H, and *erf* and *erfi* are the error and the inverse error function, respectively. The capillary pressure is then given by

$$P_c = \frac{\varsigma}{R'_H} = \varsigma 10^{\sqrt{2\sigma^2}\, erfi[1-2S_w(R'_H)] - \delta} . \tag{12}$$

Capillary pressure is specific to the nature of the two fluids involved. If no specification is made, it is understood that the displaced fluid is a vacuum. If the displaced fluid is a vacuum, and the external pressure P_c is applied in a nonwetting fluid, then all capillaries with a radius larger than R'_H will be totally filled.

CORRECTION FOR PORE ORIENTATION

In the two-dimensional sections under consideration, however, the pore cross sections are randomly oriented with respect to the directions of the channel axes. The orientation effect has been corrected by means of the following geometrical and stereological considerations (cf. Underwood, 1970), which are exact for the case of circular cross sections.

For the hydraulic radius,

$$(R_H)_{actual} = \frac{\sqrt{2}}{2}\left\langle \frac{1}{\sqrt{1+\cos^2\theta}} \right\rangle^{-1} (R_H)_{measured} , \tag{13}$$

where the brackets denote a spherical average for pores of random orientation; i.e.,

$$\left\langle \frac{1}{\sqrt{1+\cos^2\theta}} \right\rangle = \frac{\int_0^{\pi}\int_0^{\theta_{\max}} \frac{\sin\theta}{\sqrt{1+\cos^2\theta}} d\theta d\phi}{\int_0^{\pi}\int_0^{\theta_{\max}} \sin\theta d\theta d\phi} , \tag{14}$$

with $\theta_{max} = \arctan(L/D)$, where (L/D) is the maximum ratio of pore length to diameter. Using an average value of $L/D = 5$, as estimated from the micrographs, we find that

$$(R_H)_{actual} = 0.85(R_H)_{measured} . \tag{15}$$

EXPERIMENTAL APPROACH

In this experimental investigation, we have sought to examine the relationship between the microscopic pore occupancy by means of the nonwetting fluid and its effect on capillary pressure. We have used three-dimensional imbibition of a nonwetting Wood's metal alloy instead of the conventional mercury porosimetry (Schlueter et al., 1992c). This technique offers the advantage of allowing analysis of the occupied pore space after the experiment. Wood's metal is an alloy of about 43% Bi, 38% Pb, 11% Sn, and 9% Cd, with a specific gravity of 9.6, a viscosity of about 1.3×10^{-3} Pa·s at 75°C, and a surface tension of about 400 mN/m (Yadav et al., 1987). The setup for the three-dimensional imbibition experiments consists of a metallic container of Wood's metal placed in a metal vacuum chamber provided with a lucite window and surrounded by a heating element to keep the metal molten (melting point varies from about 50 to 70°C, depending on its composition). A micrometer is attached to the metallic container to determine the pressure at which the Wood's metal first enters the specimen. The 50-mm-long and 50-mm-diameter

Berea sandstone sample is first oven-dried and then immersed in the molten Wood's metal in the metallic container and placed in the metal vacuum chamber. Then the sample is de-aired by applying a full vacuum for about 60 min, until no air bubbles are observed through the lucite window. A subatmospheric pressure is applied by drawing a partial vacuum, which is maintained at the desired value by a regulating valve until capillary equilibrium is achieved. Each sample was allowed to imbibe for approximately 90 min at a fixed equilibrium pressure and until no movement of Wood's metal was noticed through the lucite window. At a pressure of about 5 to 6 psia, the micrometer signaled the first indication of Wood's metal entering the pore space (probably an edge effect on the sample sides). The capillary pressure experiment was repeated on several samples by applying pressure in the range of approximately 6 to 14 psia. The imbibed samples were cut into four axial quarters, each of which had a different saturation. To minimize the effect of gravity (hydrostatic) gradient, we took the top quarter of each imbibed specimen at a particular equilibrium pressure and measured its saturation. Figure 1 shows the experimental capillary pressure curve obtained when partially saturating the rock with the nonwetting fluid. Fluid saturation increases rather sharply with a corresponding small increase in capillary pressure in the saturation range from about 10 to 50%. Our result is consistent with typical capillary pressure curves based on conventional mercury porosimetry saturation for Berea (BE-1) sandstone (Chatzis and Dullien, 1977). Berea (BE-1) sandstone has almost the same macroscopic properties as the Berea sandstone we used in our experiments (e.g., porosity of 22%, permeability to N_2 of 400 md, and a formation factor of 15.5). Berea sandstone is a homogeneous sedimentary rock used as a reference rock in the petroleum industry. It contains about 80% quartz, 12% feldspar, and 8% by weight of dispersible and swelling clays (mainly kaolinite, with some illite and smectite). It is estimated to be of Mississippian age and is found in Berea, Ohio.

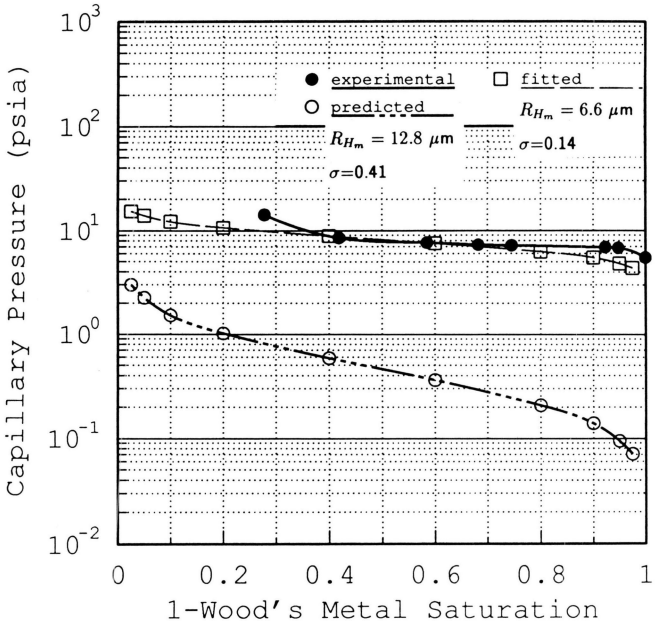

Figure 1. Experimental vs. predicted capillary pressure function for Berea sandstone. To obtain the experimental capillary pressure function, the rock has been impregnated with a nonwetting fluid (Wood's metal) at different equilibrium pressures and solidified in place. The procedure allows for direct observation and analysis of the fluid distribution at a fixed pore pressure and saturation level. [XBL 934-502]

PORE STRUCTURE AND TOPOLOGY

To understand how pore structure and topology control the physical property under consideration, we have studied the capillary pressure data in light of the nonwetting fluid distributions observed at each equilibrium pressure. For this purpose, optical and scanning electron microscopic examinations of the tops of samples (after cutting off 3 mm) have provided valuable insights into the pore-level complexity of the natural porous media. Figure 2 shows an optical photograph of the fluid distributions obtained in top axial quarters (top and bottom) in the pressure range 6.8 psia to 7.7 psia. It is observed that the nonwetting fluid flow network is composed of a set of imbibing clusters correlated in space. At every pressure step, the nonwetting fluid resides in the pores accessible through throats with a radius larger than that corresponding to the current equilibrium capillary pressure. As the pressure increases, the nonwetting phase saturation increases and the nonwetting fluid invades successively smaller pores and becomes connected to regions that were separated from this phase by small throats. Optical photographs of enlarged fluid distributions in top axial quarters obtained by partially saturating the rock with Wood's metal at equilibrium pressures of 6.8, 6.9, and 7.2 psia are presented in Figures 3, 4, and 5, respectively. At 6.8 psia (Figure 3), the fluid has preferentially penetrated the sample sides. The saturation is greatest near the perimeter of the sample and least at the center. This observation suggests that pores near the cylindrical surface of the sample are better connected than those toward the center. This interconnection could arise from exposure of pores where they intersect the surface or from damage adjacent to this surface. At 6.9 psia (Figure 4), a saturation gradation is observed in the direction of flow (preferentially horizontal). The longer flow paths are connected by smaller constrictions, so fewer flow channels are going to the sample center starting from all available channels at the sample surface. At pressures of 7.2 psia (Figure 5) and greater, the nonwetting fluid invades smaller and smaller pores, becoming connected to regions that were separated from this phase by smaller pores, and the clusters of nonwetting phase become larger and larger.

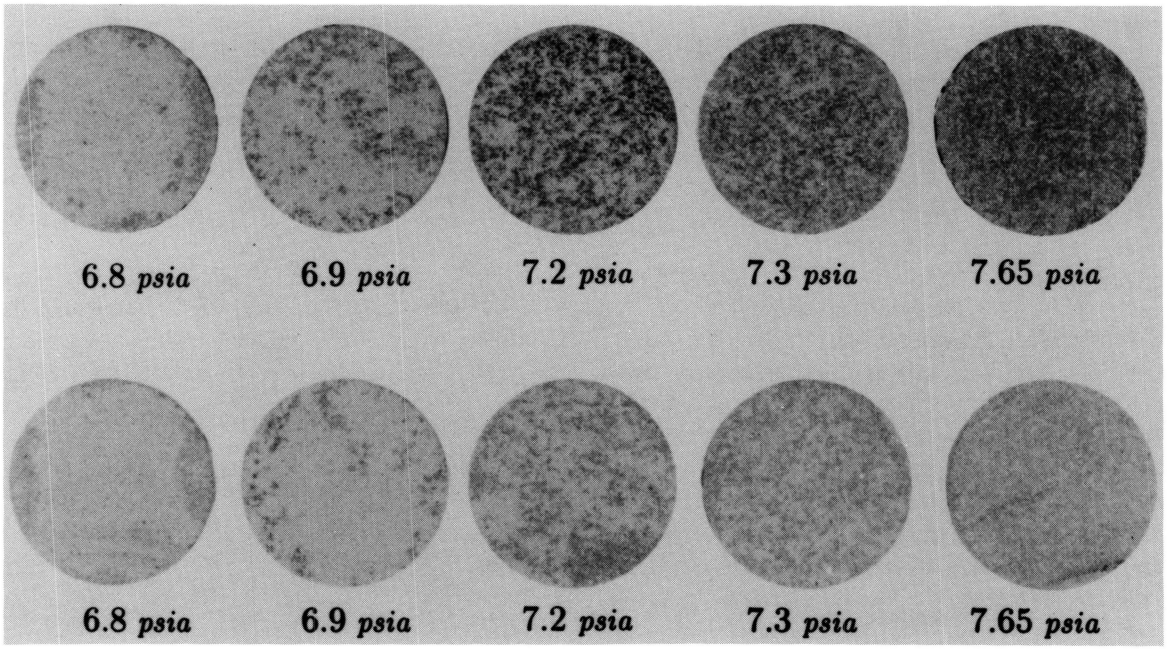

Figure 2. Top and bottom axial quarter sections of Berea sandstone core partially saturated with a nonwetting fluid (Wood's metal) at different equilibrium pressures and solidified in place. The sections reveal that the fluid distributions are composed of a set of imbibing clusters correlated in space. [CBB 919-7555]

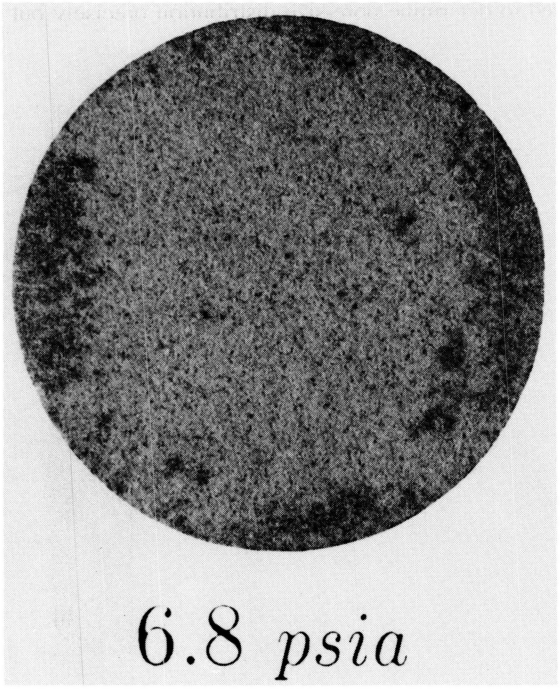

Figure 3. Top section of Berea sandstone core partially saturated with a nonwetting fluid (Wood's metal) at an equilibrium pressure of 6.8 psia and solidified in place. [CBB 910-8272]

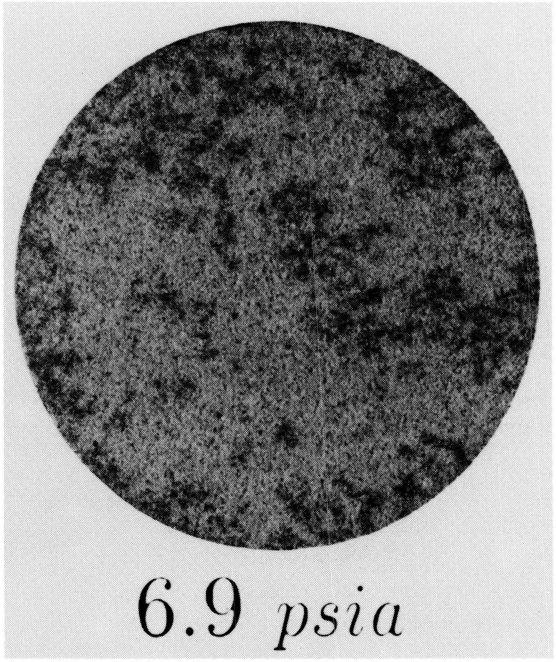

Figure 4. Top section of Berea sandstone core partially saturated with a nonwetting fluid (Wood's metal) at an equilibrium pressure of 6.9 psia and solidified in place. [CBB 910-8274]

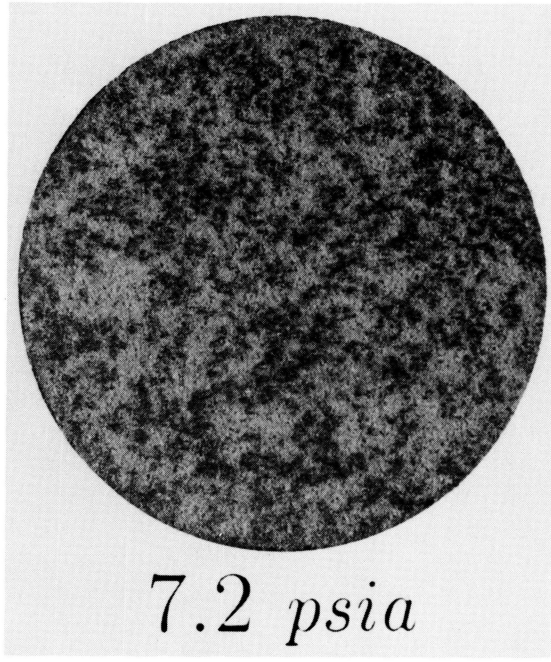

Figure 5. Top section of Berea sandstone core partially saturated with a nonwetting fluid (Wood's metal) at an equilibrium pressure of 7.2 psia and solidified in place. [CBB 910-8276]

APPLICATIONS

In this section, we calculate the predicted capillary pressure function for Berea sandstone for comparison with our experimental data. The analytical capillary pressure function for Berea sandstone has been computed using $\varsigma = 0.40$ N/m (surface tension), $\gamma = 1.49$ (perimeter-area power-law noninteger slope), $R_{H_m} = 12.8\ \mu$m (mean hydraulic radius), $\sigma = 0.41$ (standard deviation), and $(R_H)_{actual} / (R_H)_{measured} = 0.85$ (stereological correction). It is worth noting that the contours of intergranular pore space used to obtain the perimeter-area power-law relationship of pores and the distribution of pore hydraulic radii are the same contours from which the transport properties (hydraulic and electric) have been previously calculated (Schlueter et al., 1991, 1992b). Preliminary results are presented in Figure 1. As expected, the predicted capillary pressure function from such a hydraulic radius distribution does not fit the experimental capillary pressure. The photomicrographic pore-size distribution gives a good measure of the larger pore bodies, but the smaller pore throats usually remain undetected. In addition, it is generally understood that pore-size distribution determined by mercury (or Wood's metal) porosimetry does not reveal the presence of larger pore bodies and assigns their volume to pore throats. To fit the analytical to the experimental function at approximately 50% fluid saturation, a distribution represented by $R_{H_m} = 6.6\ \mu$m and $\sigma = 0.14$ is needed. An SEM photomicrograph collage of a rock specimen saturated with about 50% Wood's metal at 8.5 psia equilibrium pressure is presented in Figure 6. Simple statistical analysis of pore contour areas obtained from Figure 6 has shown that there are many intergranular pores connected by small intergranular throats that do not contribute to the flow of the nonwetting phase in the rock. In addition, the grain-contact pore space (i.e., thin sheets and micropores) does not contribute either. Therefore, a relatively small number of conduits connected by large intergranular throats carry a large fraction of the nonwetting fluid in the porous media under consideration, producing a clustered structure.

Thus our preliminary analyses show that the experimental capillary vs. saturation function (in the saturation range up to about 50%) is controlled primarily by large intergranular pore throats of narrow size distribution, represented by a mean hydraulic radius of about 6.6 μm, and a standard deviation of 0.14. This information is important because the resistance offered by the pore structure to various transport phenomena, i.e., permeability, is controlled by the pore throats.

CONCLUSIONS

Pore-size distributions and pore sizes of rocks have been measured by many researchers using a variety of methods (Dullien and Dhawan, 1974; Chatzis and Dullien, 1982; Chatzis et al., 1983; Yanuka et al., 1986; Jerauld and Salter, 1990). Most methods require a model of the pore space and simplifying assumptions. Because of these difficulties and the simplified model we use, we have not attempted to determine pore-size distribution precisely but use

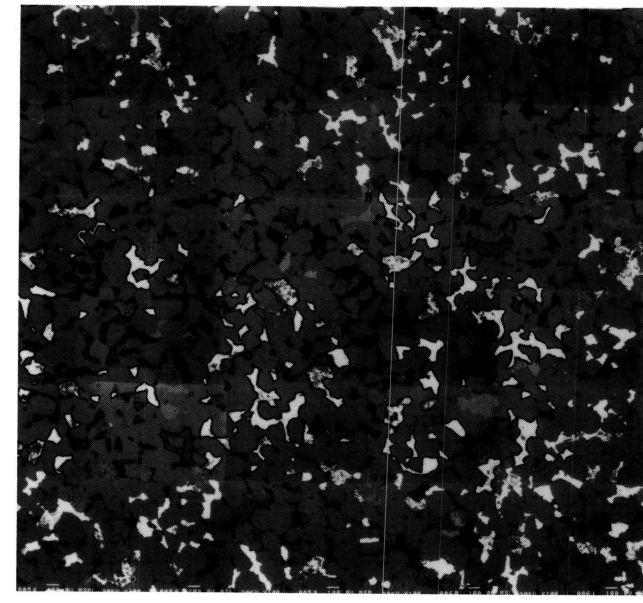

Figure 6. Scanning electron microscope photomicrograph collage of an enlarged partial section obtained from a Berea sandstone sample partially saturated with approximately 50% Wood's metal (white phase) at 8.5 psia equilibrium pressure. Actual width of the field is about 4.5 mm. [CBB 925-3596]

a simple functional form to determine average pore and throat sizes controlling capillary pressure. Our result, assuming a lognormal distribution of pore sizes, is consistent with the one obtained by Jerauld and Salter (1990), which uses an exponential pore-size distribution for Berea sandstone, and is similar to that used by Chatzis and Dullien (1982). For example, Jerauld and Salter (1990) found that pore throats are smaller than pore bodies; $r_{t_m} = 11\,\mu\text{m}$ and $r_{b_m} = 38\,\mu\text{m}$. It should be noted that the simple concept leading to Eq. (12) has several limitations, so the result is only a first approximation. For example, we have ignored possible effects due to the wetting phase being held by small-scale roughness and adsorptive forces in the pore walls, and we have neglected the effect of clay minerals, which complicates phase occupancy. Finally, the model does not account for hysteresis effects that originate from different pore accessibilities during drying and wetting cycles.

On the basis of our experimental observations of the relationship between microscopic nonwetting fluid occupancy and the fluid distributions and of their effect on capillary pressure of Berea sandstone, we have found that relatively small number of channels connected by large intergranular throats of narrow size distribution are responsible for conducting a relatively large amount of the nonwetting fluid through the medium (at least in the saturation range up to approximately 50%). In fact, we have also found that a large percentage of the permeability of the medium is contributed by a relatively small number of conduits connected by large intergranular throats of narrow size distribution and high hydraulic conductance (Schlueter et al., 1992d).

REFERENCES

Carman, P.C., 1941. Capillary rise and capillary movement of moisture in fine sands. Soil Sci., v. 52, p. 1–14.

Chatzis, I., and Dullien, F.A.L., 1977. Modelling pore structure by 2-D and 3-D networks with application to sandstones. J. Can. Pet. Technol., v. 16, p. 97–108.

Chatzis, I., and Dullien, F.A.L., 1982. Application of the theory of percolation for a model of drainage in porous media and relative permeability of injected nonwetting liquid. Rev. l'Institut Francais du Petrole, v. 37, p. 183–205.

Chatzis, I., Morrow, N.R., and Lim, H.T., 1983. Magnitude and detailed structure of residual oil saturation. Soc. Pet. Eng. J., April, p. 311–326.

Dullien, F.A.L., and Dhawan, G.K., 1974. Characterization of pore structure by a combination of quantitative photomicrography and mercury porosimetry. J. Coll. Int. Sci., v. 47, p. 337–349.

Jerauld, G.R., and Salter, S.J., 1990. The effect of pore structure on hysteresis in relative permeability and capillary pressure: Pore-level modeling. Transport in Porous Media, v. 5, p. 103–151.

Pruess, K., and Tsang, Y.W., 1989. On relative permeability of rough-walled fractures. Lawrence Berkeley Laboratory Report LBL-26509.

Scheidegger, A.E., 1974. The Physics of Flow through Porous Media. University of Toronto Press.

Schlueter, E., and Pruess, K., 1990. Sensitivity studies on parameters affecting gas release from an underground rock cavern. Lawrence Laboratory Report LBL-28818.

Schlueter, E., Zimmerman, R.W., Cook, N.G.W., and Witherspoon, P.A., 1991. Predicting permeability and electrical conductivity of sedimentary rocks from microgeometry. *In* Proceedings, 32nd U.S. Symposium on Rock Mechanics, A.A. Balkema, Rotterdam, p. 355–364.

Schlueter, E., Myer, L.R., Cook, N.G.W., and Witherspoon, P.A., 1992a. Formation factor and the microscopic distribution of wetting phase in pore space of Berea sandstone. Lawrence Berkeley Laboratory Report LBL-33207.

Schlueter, E., Zimmerman, R.W., Cook, N.G.W., and Witherspoon, P.A., 1992b. Perimeter-area power-law relationship of pores in sedimentary rocks and implications for permeability. *In* Earth Sciences Division Annual Report 1991. Lawrence Berkeley Laboratory Report LBL-31500.

Schlueter, E., Zimmerman, R.W., Myer, L.R., Cook, N.G.W., and Witherspoon, P.A., 1992c. Predicting the capillary pressure of sedimentary rocks from microgeometry. Lawrence Berkeley Laboratory Report LBL-33830.

Schlueter, E., Myer, L.R., Cook, N.G.W., and Witherspoon, P.A., 1992d. Residual permeability and the distribution of wetting and non-wetting phases in pore space of Berea sandstone. Abstract presented at the 29th Annual Technical Meeting of the Society of Engineering Science, La Jolla, California. Lawrence Berkeley Laboratory Report LBL-32564A.

Schultze, K., 1925a. Kapillarität, Verdunstung, und Auswitterung. Kolloid Ztschr., v. 36, p. 65–78.

Schultze, K., 1925b. Kapillarität und Benetzung. Kolloid Ztschr., v. 37, p. 10–17.

Underwood, E.E., 1970. Quantitative Stereology. Addison-Wesley, Reading, Massachusetts.

Yadav, G.D., Dullien, F.A.L., Chatzis, I., and Macdonald, I.F., 1987. Microscopic distribution of wetting and nonwetting phases in sandstones during immiscible displacements. SPE Res. Eng., May, p. 137–147.

Yanuka, M., Dullien, F.A.L., and Elrick, D.E., 1986. Percolation processes and porous media: I. Geometrical and topological model of porous media using a three-dimensional joint pore size distribution. J. Coll. Int. Sci., v. 112, p. 24–41.